Metastatic colorectal cancer cells maintain TGFβ program and use TGFBI to fuel angiogenesis

Barbara Chiavarina *[1,2,3,4], Brunella Costanza[5]*, Roberto Ronca[6], Arnaud Blomme[5], Sara Rezzola[6], Paola Chiodelli[6], Ambre Giguelay[1,2,3,4], Guillame Belthier[2,4,7,8], Gilles Doumont[9], Gaetan Van Simaeys[9,10], Simon Lacroix[9,10], Takehiko Yokobori[11], Bilguun Erkhem-Ochir[11], Patrick Balaguer[2,3,4,12], Vincent Cavailles[2,3,4,12], Eric Fabbrizio[2,3,4,13], Emmanuel Di Valentin[14], Stephanie Gofflot[15], Olivier Detry[16], Guy Jerusalem[17], Serge Goldman[9,10], Philippe Delvenne[18], Akeila Bellahcène[5], Julie Pannequin[2,4,7,8], Vincent Castronovo[5]† and Andrei Turtoi[1,2,3,4,11]†

[1]Cancer Research Institute of Montpellier, Tumor Microenvironment Lab, Montpellier, France.

[2]Institut National de la Santé et de la Recherche Médicale, Montpellier, France.

[3]Institut du Cancer de Montpellier, Montpellier, France.

[4]Université de Montpellier, Montpellier, France.

[5]Metastasis Research Laboratory, GIGA Cancer, University of Liège, Liège, Belgium.

[6]University of Brescia, Department of Molecular and Translational Medicine, Brescia, Italy.

[7]Institut de Génomique Fonctionnelle, Montpellier, France.

[8]Centre National de la Recherche Scientifique, Montpellier, France.

[9]Center for Microscopy and Molecular Imaging (CMMI), Université libre de Bruxelles (ULB), rue Adrienne Bolland 8, B-6041 Charleroi (Gosselies), Belgium.

[10]Nuclear Medicine department, ULB Hôpital Érasme, route de Lennik 808, B-1070 Brussels, Belgium.

[11]Gunma University Initiative for Advanced Research, International Open Laboratory, Universities of Liege and Montpellier Lab, Gunma University, Gunma, Japan.

[12]Cancer Research Institute of Montpellier, Hormon Signaling and Cancer Lab, Montpellier, France.

[13]Cancer Research Institute of Montpellier, Oncogenic Pathways in Cancer Lab, Montpellier, France.

[14]GIGA-Viral Vectors Platform, University of Liège, Liège, Belgium.

[15]BIOTHEQUE, University of Liege, Liege, Belgium.

[16]Department of Abdominal Surgery, University Hospital, University of Liège, Liège, Belgium.

[17]Department of Medical Oncology, University Hospital, University of Liège, Liège, Belgium.

[18]Department of Pathology, University Hospital, University of Liège, Liège, Belgium.

Running title: TGFBI expression fuels angiogenesis in CRC metastases.

Disclosure of Potential Conflicts of Interest: Authors have no conflict of interest to disclose.

* Equal contribution

† Corresponding Authors:

Andrei Turtoi, PhD

Email: andrei.turtoi@inserm.fr

Vincent Castronovo, MD, PhD

Email: vcastronovo@uliege.fr

ABSTRACT

Colorectal cancer (CRC) cells are traditionally thought to be unresponsive to TGFβ due to mutations of the receptor or/and downstream signaling. CRC cells have been shown to benefit from TGFβ only indirectly, via stromal cells such as cancer-associated fibroblast. The ability of CRC cells to directly respond to TGFβ remains unexplored/underestimated and as such a missed opportunity for diagnostic and therapeutic intervention.

Methods: We examined the ability of CRC cells from both primary and metastatic tumors to respond to TGFβ via the induction of TGFβ-induced protein ig-h3 (TGFBI). The contribution of canonical and non-canonical TGFβ signaling was examined *in vitro*, while the impact of TGFBI on metastasis and angiogenesis was examined both *in vitro* and *in vivo*. Novel antibodies against TGFBI were raised and their diagnostic/ tumor-targeting value was examined on patient sera and in the mouse model of CRC liver metastasis.

Results: We show for the first time that metastatic CRC cells, such as circulating tumor cells, maintain TGFβ responsiveness. They are characterized by absence of TGFβ receptor mutations and frequent presence of p53 mutations. The pro-tumorigenic program orchestrated by TGFβ in CRC cells is facilitated by TGFBI, whose expression was positively regulated by non-canonical TGFβ signaling. Inhibition of TGFBI was sufficient to significantly reduce liver metastases *in vivo*. We further show that pro-tumorigenic function of TGFBI stems from its ability to stimulate angiogenesis. Levels of TGFBI in sera of CRC patients were higher than in normal individuals and were significantly reduced by chemotherapy. Systemically injected radiolabeled TGFBI antibody selectively targeted metastatic deposits *in vivo*, underscoring the value of this target for both diagnostic and therapeutic purposes.

Conclusions: TGFβ program in CRC cells is not a marginal event, but it rather assures their metastatic capacity and stromal-independence. Proteins resulting from activated TGFβ-signaling, such as TGFBI, represent novel diagnostic and therapeutic targets allowing for more specific anti-metastatic therapies.

Key words: alternative TGFβ signaling, liver metastases, endothelial cells.

INTRODUCTION

Colorectal cancer (CRC) is the third most frequent cause of cancer-related death worldwide, and is usually lethal when associated with liver metastases. Unfortunately, 40% of CRC patients have metastatic deposits in the liver at the time of diagnosis [1]. Our ability to treat metastases is thus the most important aspect of the medical care for CRC patients. Despite decades of research the process of tumor dissemination is insufficiently understood precluding the development of metastasis-specific treatments. It is clear that only a subpopulation of tumor cells is responsible for metastases and among those circulating tumor cells (CTC) are considered as the most probable actors [2, 3]. To make the issue more complex, not only cancer cells, but tumor microenvironment (TME) as well plays an important role. While the cells of the TME have been traditionally considered as accomplices to cancer cells [4], we know today that TME is also an important barrier for tumor development [5]. Early metastatic cells arrive in all but friendly environment and thus require plasticity, especially until tumor-promoting paracrine interactions with the stroma have been established.

TGFβ and its signaling machinery are important if not the most essential mediators of cancer cell plasticity [6]. Paradoxically, TGFβ signaling switches the function from tumor-suppressor to tumor-promoter, in particular during colon cancer progression. TGFβ signaling in epithelial colonic cells synergizes with NOTCH pathway to counteract APC mutation-induced Wnt hyperactivation [7]. Today it is widely accepted that transformation of APC mutated cells ultimately requires their unresponsiveness to TGFβ signaling that is often achieved through SMAD4 or/and TGFβ-receptor mutations. It is further established that TGFβ stimulates CRC progression mainly through cancer-associated fibroblasts (CAF) [8]. CAF supply a plethora of TGFβ-induced factors, such as MMPs, PDGF, CTGF, etc., that colon cancer cells necessitate to survive, proliferate and invade [9, 10]. The majority of colon cancer cells certainly require the paracrine interaction with CAF. However, when thought at the level of the metastatic cells, inability to respond to TGFβ-stimulus would make these cells particularly vulnerable. They would not benefit from the TGFβ-orchestrated autocrine signaling that helps maintain their ability to adapt to the new environment. One thus asks the question whether some CRC cells could maintain TGFβ-responsiveness despite inactivating mutations in the canonical TGFB-signaling machinery. Indeed, this could be achieved via alternative SMAD independent pathways (e.g. ERK, p38) that are intact in most cancer cells [9, 10]. Mutations of TGFβ-receptors are also not absolutely prohibitive for the downstream signaling. Studies have demonstrated that despite some frame-shift mutations, the resulting TGFBR2 protein can remain functional [11]. Nonetheless, TGFβ-

responsive cancer cells represent the minority of CRC cell universe and their existence and phenotype remains to date debatable and unknown.

To gain a better insight into the TGFβ-mediated pro-metastatic program in CRC cells we have investigated the expression pattern and function of a major TGFβ-induced protein, TGFBI. *TGFBI* has been cloned as *TGFβ*-inducible gene in lung adenocarcinoma cells [12]. TGFBI contains 4 FAS1 domains, which are thought to represent cell adhesion domains conserved between plants and animals [13]. The 4th FAS1 domain of TGFBI contains also an RGD motif that has a strong affinity to integrins [14]. A wealth of literature exist on TGFBI function in solid cancer, most of which has been recently reviewed by Yokobori & Nishiyama [15]. Despite this richness of data, there is a significant lack of consensus whether and in which context is the function of TGFBI pro- or anti-tumorigenic. For example, Zhang et al. [16] showed that TGFBI null animals developed rapidly lung and liver malignancies. Opposite to this, Ma et al. [17] demonstrated that overexpression of TGFBI in colon cancer cells enhanced liver metastases. Paradoxically, very few studies on TGFBI have connected its function with TGFβ activity. However, the fact that TGFBI is modulated by TGFβ-program renders the function of this protein (tumor promoting or suppressing) cell and context dependent. In the present study we therefore show that TGFBI produced by cancer cells following their activation by TGFβ, fuels angiogenesis and thus assumes a pro-metastatic function. This finding puts forward TGFBI as a novel therapeutic target that is downstream of TGFβ, eliminating the need to target the entire pathway and rather focus on specific, metastasis-promoting components.

MATERIALS AND METHODS

Human samples

The ethical committee of the University Hospital Liege approved the use of human material in the present study. All samples were obtained from the institutional Biobank. Patients obtained the information that the residual material could be used for research purpose and the consent is presumed as long as the patient does not oppose (opting-out in line with Belgian law). For serum measurement of TGFBI levels, 14 normal human individuals along with 17 colorectal cancer patients were enrolled. Treatment information and patient status are given in **Table S1**. For immunohistochemistry analysis, 78 colorectal cancer (**Table S2)** and 21 colorectal cancer liver metastases (**Table S3**) patients were included. When available adjacent normal tissue was evaluated as control.

Immunohistochemistry

Formalin-fixed paraffin-embedded (FFPE) tissue sections were prepared from primary CRC and CRC-liver metastases lesions. Five μm thick paraffin sections were deparaffinized three times in xylene for 5 min and hydrated in a methanol gradient (100%, 95%, 70%, and 50%). Blocking of unspecific peroxidase activity was performed for 30 min with 3% H_2O_2 and 90% methanol. Following antigen retrieval step (citrate buffer pH6, 95 °C, 40 min), tissues were blocked with Protein Block Serum-Free solution (Protein Block Serum-Free Ready-to-Use, catalog no. X0909, Dako, Glostrup, Denmark) for 30 min at room temperature, and incubated with 1:200 dilution of anti-TGFBI (Cell Signaling, Danvers, USA; catalog no. 2719) overnight at 4 °C. Next, samples were washed in PBS and incubated with Histofine MaxPo-Multi HRP-polymer (Nichirei, Tokyo, Japan; cat. no. 414152F) for 30 min. Sections were washed three times for 5 min in PBS and then stained with 3,3'-diaminobenzidine solution (Agilent-Dako, cat. no.: GV800). The slides were counter-stained with hematoxylin (Sigma Aldrich, cat. no.: MHS32) and mounted with Eukitt (Orsatech GmbH, Bobingen, Germany). Scoring of protein expression was performed in accordance with the previously published methodology [18]. Briefly, each IHC slide was assessed for the intensity of the staining using the following scale: 0 = no staining, 1 = weak, 2 = moderate and 3 = strong. The tissue was further evaluated for the extent of positivity (percent positive area) using the following scale: 0 = 0%–25%, 1 = 25%–50%, 2 = 50%–75% and 3 = 75%–100%. The values obtained by each of the two scales were multiplied to yield a composite value called the IHC score. Pictures of representative fields were taken under a Leica DMRB light microscope (Leica, Wetzlar, Germany). Two independent pathologists scored the samples using the above method and average scores were reported.

Immunofluorescence

Paraffin removal, antigen retrieval and blocking steps were performed as described above. The sections were then washed three times using Tris-buffered saline with 0.05% Tween-20 (TBS-T) and then incubated ON at 4 °C with 1st antibody, anti-TGFBI or anti-murine IgG (Sigma-Aldrich; catalog no. M5284). Following 5 wash steps at 5 min each, the slides were incubated with Histofine MaxPo-Multi HRP-polymer for 30 min at RT. After additional 5 wash steps, the signal was revealed using 100 μL stain solution prepared from 2 μL Opal dye and 98 μL Amplifying Buffer (Perkin Elmer, Waltham, MA, USA; cat. no.: NEL810001KT). Following 10 min incubation, the slides were washed and subjected to microwave-assisted antibody removal (as described by the manufacturer). After new blocking step, sections were either counterstained and mounted (anti-murine IgG) or incubated with the next antibody overnight at 4 °C. Following antibodies were used subsequently (all at 1:1000 dilution): anti-VIM (Cell Signaling; catalog no.

57415) and anti-panCK (Abcam; catalog no. ab24647). After incubation with the 3rd antibody and staining with Opal dye, slides were washed and mounted using VECTASHIELD® Antifade Mounting Medium with DAPI (Vector, Burlingame, USA). Images were accrued using Zeiss Apotome microscope (Zeiss, Oberkochen, Germany).

Cell culture

Human colorectal cancer cell lines LS174T, LOVO, HT29 and HCT116 cells were obtained from ATCC (Virginia, USA). SW1222 colon carcinoma cells were a kind gift of Prof. W. Bodmer, Department of Medical Oncology, Weatherall Institute, Oxford, UK. HT29-LM and HT29-HM were a kind gift of Dr. Raffaella Giavazzi, Institute Mario Negri, Milano, Italy. Human normal colon fibroblasts CCD-18Co were obtained from ATCC. All cells were cultured in enriched medium (Dulbecco's Modified Eagle medium supplemented with 10% fetal bovine serum; Gibco, Invitrogen, Life Technologies, Carlsbad, CA, USA) at 37 °C in a 5% CO_2 atmosphere. Additionally, to the WT cells, SW1222 cells depleted for *TGFBI* expression were generated using lentiviral shRNA particles. The latter was obtained from Sigma Aldrich (St. Louis, MO, USA; cat. no.: TRCN0000062177 (#1) and TRCN0000062175 (#2)). Control shRNA was anti-eGFP shRNA plasmid (Sigma; cat. no.: SHC005). All shRNA were inserted into the pLenti6/V5 using the pLenti6/V5 Directional TOPO® Cloning Kit (Invitrogen, Carlsbad, CA, USA), Part # K4955-00). Lentiviral vectors were obtained by co-transfection of Lenti-X™ 293T Cell Lines (Clontech, Mountain View, CA, USA; Part # 632180) with pLenti6-Luciferase, psPAX2 (Addgene, Cambridge, MA, USA; Part #12260) and pVSV-G plasmids. Viral supernatants were collected, 48 h - 96 h post transfection, and filtered (0.45 µm). SW1222 cells were incubated with these lentiviral particles for 48 h and subsequently subjected to puromycin selection at 1 µg/mL (Sigma Aldrich, St. Louis, MO, USA). Primary human umbilical vein endothelial cells (HUVEC) were used at early passages (passages II–V) and grown on plastic surface coated with porcine gelatin in M199 medium (Invitrogen, Carlsbad, CA, USA) supplemented with 20% fetal calf serum (Invitrogen), 100 µg/mL endothelial cell growth factors (Sigma-Aldrich, St. Louis, MO, USA), and 100 µg/mL porcine heparin (Sigma-Aldrich, St. Louis, MO, USA). CTC, primary and metastatic CPP were isolated, established as previously described [19, 20]. They were maintained in 1 mL of M12 medium (using ultralow attachment 24-well plates (Corning). The M12 medium contained DMEM-F12 (Gibco), 2 mmol/L of L-glutamine (Gibco, Thermo Fisher Sci., Waltham, MA, USA), 100 unit/mL of penicillin and streptomycin (Gibco, Thermo Fisher Sci., Waltham, MA, USA), N2 supplement (Gibco, Thermo Fisher Sci., Waltham, MA, USA), 20 ng/mL of epidermal growth factor (R&D Systems, Minneapolis, MN, USA) and 10 ng/mL of fibroblast growth factor-basic (R&D Systems, Minneapolis, MN, USA).

Conditioned medium (CM) from colorectal cancer cell lines was obtained after 48 h incubation of 80% confluent cells in serum-free medium. Cells CM were collected, centrifuged for 5 min at 150xg, room temperature, and then added to fibroblast monolayer (cells were pre-starved in serum-free medium for 6 h) for an additional 48 h. Following this, fibroblast monolayers were washed two times with PBS and then lysed for Western blot analysis. For TGF-β1 treatment, eighty percent confluent cells were starved in serum-free media for 16 h and then treated for 48 h with 5 ng/ml of recombinant TGF-β1 (Roche, catalog no. 11412272001) in serum-free medium. The treatment was repeated every 24 h.

Human SMAD2 siRNA (ON-TARGETplus SMARTpool Human SMAD2 (4087)) and scrambled siRNA (ON-TARGETplus NonTargeting Control Pool, catalog no. D-001810-10-05) were purchased from Dharmacon. Transfection of cultured SW1222 cells with 20 nM of each siRNA was performed using Lipofectamine (Lipofectamine 2000 reagent, catalog no. 11668-019, Life Technologies, Carlsbad, CA, USA).

The following compounds were used to treat the cells: SB202190 (5 µM, catalog no. S7067, Sigma-Aldrich), BAY11-7082 (5 µM, catalog no. B5556, Sigma-Aldrich), SP600125 (5 µM, catalog no. S5567, Sigma-Aldrich), MK2206 (1 µM, catalog no. 1032350-13-2, Santa Cruz Biotechnology, Dallas, TX, USA), PD98059 (5 µM, catalog no. 19-143, Merck Millipore, Burlington, MA, USA), ARRY-614 (10 µM, catalog no. S7799, Selleckchem), LY2228820 (5 µM, catalog no. A413122, Sigma-Aldrich).

Cell line mutation analysis

Mutational status of the different commercially available CRC cell lines was derived from the public database COSMIC (https://cancer.sanger.ac.uk/cosmic). The mutation status of CTC44 and CTC45 cells used in the present study was derived from the previously published and deposited RNAseq data (BioProject no.: PRJNA384289).

Western blot analysis

Crushed snap-frozen tissue or cell pellets were extracted using RIPA buffer (150 mM NaCl, 0.5% Na-deoxycholate, 1% Triton X-100, 0.5% SDS, 50 mM Tris-HCl (pH 7.5)) and protease/phosphatase inhibitor cocktails (catalog no. 16829900; Sigma-Aldrich). Protein lysates of all samples were quantified using the Pierce BCA Protein Assay Kit (Thermo Scientific; catalog no. 23225). Twenty micrograms of proteins were supplemented with Laemmli buffer (0.1% 2-mercaptoethanol, 0.0005% bromophenol blue, 10% glycerol, 2% SDS in 63 mM Tris-HCl (pH 6.8)), boiled for 5 min and loaded on 10% polyacrylamide gel. Proteins were transferred to nitrocellulose membranes for 2 h at 100 V. After blocking in 5% skim milk, membranes were

incubated with the primary antibody (overnight, 4 °C). The following antibodies were used: 1:500 dilution anti-TGFBI (Cell Signaling; catalog no. 2719), 1:1000 dilution anti-SMAD2/3 (Cell Signaling; catalog no. 8685,) and 1:10000 dilution anti-beta-actin (Cell Signaling; catalog no. 4967). Beta-actin was used as a normalizator.

In vitro assays on HUVEC

Tumor cells (50,000/cm^2) were seeded in complete medium. After 24 hours, cells were washed and grown in absence of serum with or without the addition of 20 μg/ml recombinant TGFBI or 20 μg/ml of the anti-TGFBI antibodies (4G6 and 10G9). The conditioned media were collected, filtered and used for the *in vitro* assays. Proliferation assay: HUVECs (15,000/cm^2) were treated with conditioned media (100%) in the presence of 2.5% FCS. 24 hours later, cells were detached and counted with a MACSQuant cytofluorimeter (Milteny Biotec). Sprouting assay: HUVEC spheroid aggregates were embedded in fibrin gel and stimulated with 50% of conditioned media in the presence of 5% FCS. After 24 hours, growing cell sprouts were photographed and counted under an inverted microscope (Carl Zeiss Vision GmbH). Wound repair assay: HUVEC monolayers were scratched with a 200 μL tip to obtain a 2-mm-thick denuded area and cultured in the presence of 100% conditioned media with 3.5% FCS. After 18 hours, wounded monolayers were photographed and the percentage of repaired area was quantified with Fiji software [21].

In vivo models of CRC

Chicken-chorioallantoic membrane (CAM) *in vivo* colorectal carcinoma tumor model was based on SW1222 cells as previously described [22]. CAM were implanted on embryonic day 11 with 2×10^6 cancer cells suspended 1:1 in culture medium with Matrigel (BD Biosciences, Bedford, MA) (100 μl final volume). Tumor volume was estimated assuming the ellipsoid shape and using the formula V= 4/3.π.((l.w.h)/8), where l, w, h represent the length, width and height of the tumor.

Orthotopic model of CRC liver metastases was performed using SW1222, HT29 and HCT116 cells that were injected intra-spleen in NOD-SCID mice (Janvier Labs, Saint Berthevin Cedex, France). All experimental procedures used in the current work were performed in accordance with the ARRIVE ethical guidelines [23]. They were reviewed and approved by the Institutional Animal Care and Ethics Committee of the University of Liège (Belgium). The experimentation adhered to the "Guide for the Care and Use of Laboratory Animals" prepared by the Institute of Laboratory Animal Resources, National Research Council, and published by National Academy Press, as well as to European and local legislation. Mice were anesthetized using 75 mg/kg of Ketamine (CEVA, Bruxelles, BE) and 10 mg/kg of Xylazine (Rompun®, Bayer, Diegem, BE), spleen was surgically exposed and injected with 500.000 cells in 100 μL saline solution with 5

mM EDTA. Following the splenic injection of cancer cells, development of metastatic deposits in the liver was assessed after 6 weeks at necropsy.

ELISA assay on human sera

Homemade sandwich ELISA assay was used to quantify TGFBI levels in sera samples. MaxiSorp 96 microtiters plates (Nunc, GmbH, Germany) were coated with 100 μL of TGFBI antibody (clone 4G9A10, Targetome SA), at a concentration of 1 ug/mL in carbonate buffer, and incubated overnight at 4 °C. The coated wells were washed three times with PBS-tween (0.05%) and blocked with 200 μL of 10% FBS-PBS for 2 h at 37 °C. Microtiter plate was then washed three times as described above and filled with 100 μL of samples/well. Serial dilution of human Recombinant TGFBI (Targetome SA) in a range varying from 0 μg/mL to 5 μg/mL was prepared in PBS to serve as a calibration curve. Patient sera were diluted 1:20 in PBS. Following this, the plate was incubated for 1 h at 37 °C. After washing, the wells were incubated with 100 μL of TGFBI antibody (Dilution 1:500 in 10% FBS-PBS; clone 4G6B10, Targetome SA) for 1 h at 37 °C. Microtiter plate was washed as described above and to the samples 100 μL of anti-mouse antibody (Dako; cat. no. P0260) at a dilution of 1:3000 in 10% FBS-PBS was added. The samples were then incubated for 1 h at 37 °C. Following a washing step, optical density was measured after incubation with 30% H_2O_2-ABTS (1 mM; 2,2'-Azinobis-[3-ethylbenzothiazoline-6-sulfonic acid] solution, using Filter Max F5 plate reader (Molecular Devices, Sunnyvale, CA, USA) at 405 nm.

[89]Zr-radiolabeling of the monoclonal antibodies targeting TGFBI

The radiolabeling of the TGFBI antibody was performed in a three-step procedure accordingly to the previously published method [24]: (1) the coupling of the antibody with a chelate, the p-isothiocyanatobenzyl-desferrioxamine, (2) the radiolabeling of the chelated antibody with [89]Zr oxalic acid and (3) the purification by exclusion chromatography on a Sephadex G25 matrix. Radiolabeling yield and volume activity were assessed. Thin layer chromatography (TLC) was then performed to check the absence of free [89]Zr contamination in the radiolabeled antibody solution. Finally, antigen-binding properties of radiolabeled TGFBI antibody were evaluated by ELISA assay.

PET/CT imaging of anti-TGFBI bio-distribution

Orthotopic mouse models based on TGFBI expressing HT29 cells and TGFBI negative HCT116 cells were made as described above. Mice were injected with a contrast product (Exitron® nano12000, Miltenyi Biotec, Germany; 50 ul/mouse) to highlight the liver and the

spleen on X-ray computed tomography (CT) imaging. One hundred μg of 89Zr-radiolabeled 4G6B10 TGFBI antibody were injected intravenously in 10 mice/model aiming at 4-5MBq/mouse at the time of injection. PET/CT imaging was performed on a preclinical nanoScan PET/CT scanner (Mediso, Hungary). The mice were anaesthetized with isoflurane gas for the duration of the examination (induction: 4l O_2/min, 3.5% isoflurane; maintenance: 1.5 l O2/min, 1.75% isoflurane). PET imaging was performed at 2 days (D2, 30 min scan), 6 days (D6, 30 min scan) and 13 days (D13, 45 min scan) post injection of radiolabeled antibodies. PET emission data were recorded in 3-to-1 coincidence mode in normal count rate. PET acquisitions were reconstructed with a fully three-dimensional iterative algorithm (TeraTomo from Mediso, with 4 iterations, 6 subsets, normal regularization setting, median filtering period defined from iteration counts, and spike filter) to get a voxel size of 0.4 mm ("normal" mode). Each PET scan was followed by a 6-minute CT scan for anatomical localization, as well as attenuation and scatter correction of PET images. CT acquisition parameters were 50 kV for a tube current of 520 μA, 300 ms per projection, 480 projections per rotation, a 4-to-1 frame binning, and a cubic reconstructed voxel size of 251 μm. All PET images were also corrected for random counts, dead time and decay. Viewing and quantitative analysis of PET-CT images of mice injected with 89Zr-radiolabeled 4G6B10 and 89Zr-radiolabeled 18D4H1 were performed using VivoQuant v2.5 (InVicro, MA, USA).

Statistical analysis

Unless otherwise indicated, statistical analysis was performed from 3 biological replicates using a two-sided, unpaired Student's *t*-test, assuming equal variances and employing GraphPad Prism (GraphPad Software, Inc., La Jolla, CA, USA; version 5.01). The *t*-test was used when data followed a normal distribution (Shapiro-Wilk test, threshold 0.05). Immunoblots were quantified by densitometric analysis using Image J software and normalized using ACTB. For IHC evaluation, box-plots were generated using Sigma Plot software (Systat Software Inc., Chicago, IL, USA; version 11.0). For the number of individuals involved in those studies refer to figure legend. Testing of statistical significance for IHC data was performed using Mann-Whitney-U-test because the data did not follow the normal distribution (Shapiro-Wilk test, threshold 0.05).

RESULTS

TGFBI expression is predominantly stromal in primary CRC, while it is detectable in cancer cells of matched metastases. In order to further understand the expression pattern of TGFBI in CRC we have initially performed a screen in 5 pairs of matched primary tumor/liver metastasis samples, including normal colon. As shown in the **Figure 1A**, regardless of the TGFBI

expression in the primary tumor (2 cases out of 5 are nearly negative), TGFBI is always highly expressed in CRC liver metastasis. To better delineate the source of expression variability, we further sought to examine TGFBI levels in histological sections of CRC and CRC-LM (**Figure 1B**). In the primary tumor, 12 out of 78 patients had low (score 2-4) or no TGFBI expression while the majority had medium to high expression (score 6-9). As far as the metastases are concerned, all but one patient had high TGFBI expression. Normal adjacent colon and normal adjacent liver showed low or no staining (low positivity was limited only to normal stroma). Representative IHC images are provided in the Supplemental Data **Figure S1A-B**. The discrepancy between the primary tumor and metastasis stemmed mainly from the observation that in the primary tumor only tumor stroma was positive for TGFBI, while in the metastasis cancer cells were also frequently positive (**Figure 1C**). Stromal positivity remained however predominant. As far as subcellular localization is concerned, TGFBI expression in the epithelial cancer cells was limited to the cytoplasm/plasma membrane and peri-nuclear space. In the cancer stroma, fibroblast cytoplasm was strongly positive as well as extracellular areas within the zone of desmoplastic reaction. This was in line with the literature evidence/and our data that TGFBI is a secreted protein (**Figure S1C**). To better understand why some CRC cells express TGFBI while others do not, we next sought to examine the status of TGF-β signaling in a panel of CRC cells as well as normal colonic fibroblasts.

TGFβ-signaling is active in TGFBR wild-type cancer cells. To obtain an overview of TGFβ-signaling in colon cancer cells and colon fibroblasts we have assembled a panel of commercially available cell lines and tested their basal TGFBI expression (**Figure 2A**). Among the cell lines tested, only HT29 and SW1222 CRC cells as well as CCD-18Co colonic fibroblasts have detectable basal levels of TGFBI. The screening indicated that compared to HT29 parental clone (HT29pt), TGFBI expression is higher in the highly metastatic derivative of HT29 cells (here called HT29hm) while it is lower in the low metastatic derivative (HT29lm) [25]. As far as the fibroblasts are concerned, the expression of TGFBI is increased following their exposure to the conditioned media of all CRC cancer cells studied here. Knowing that TGFBI status is indicative of TGFβ-signaling, we next sought to test if exposure of different cancer cells to TGF-β1 could induce TGFBI expression. As shown in the **Figure 2B**, of all the cell lines tested, only SW1222 and HT29 (all clones), were responsive to TGF-β1. Next to this, we also examined primary circulating tumor cells isolated from the blood of CRC patients. All CTCs tested positive for TGFBI expression and were also responsive to TGF-β1 exposure. A closer look at the status of TGFβ signaling in terms of possible mutations, gave a potential explanation for the observations made above (**Figure 2C**). Namely, HCT116 and LS174T cells that did not respond to TGF-β1 have frame shift (fs) mutations in the TGFβ receptor. LOVO cells had mutation in the

SMAD2. While the latter is not indispensable for TGFβ signaling, LOVO cells did not appear to respond to TGF-β1 at least with respect to TGFBI expression. All the responder cells in our hands, including CTC44 and CTC45 (for which sequencing data were available; BioProject PRJNA384289) had no mutations in the TGFβ receptor or SMAD2. They were however mutated for SMAD4, which is a mandatory downstream protein for canonical TGF-β1 signaling. Interestingly, the strongest responders such as HT29 and CTC cells had additionally p53 mutations. This was particularly relevant because p53 has been described as mediator of TGFβ signaling in conjunction with SMAD2 in human hepatocarcinoma HepG2 cells and mouse embryonic fibroblasts [26]. We have next sought to explore this link in the CRC context by several means. First, we have silenced the mutant p53 (R273H) in HT29hm cells and verified if these responded differently to TGF-β1. No significant modulation of TGFBI was observable between control and p53 silenced HT29hm cells following their challenge with TGF-β1 (**Figure S2A-B**). Silencing of WT p53 (present at very low protein expression levels; data not shown) in SW1222 cells resulted in no modification of the response to TGF-β1 challenge (**Figure S2C-D**). Introduction of mutant p53 (R273H) in SW1222 cells did result in stronger TGFBI expression upon the treatment of these cells with TGF-β1 (**Figure S2E**). However, this augmented responsiveness was to a large extent due to an increase of basal TGFBI expression upon the introduction of the mutant p53 in the SW1222 cells.

In order to further confirm that TGFβ signaling (and hence TGFBI expression) is stronger in metastatic CRC cells compared to ones isolated from primary tumors, we turned next to a set of primary cells isolated from CRC tumors and metastases (**Figure 2D**). In line with the previous observation, all cancer cells derived from CRC liver metastases expressed TGFBI. This was in sharp contrast to primary tumor cell lines that had no detectable levels of this protein. Metastatic cells that had low TGFBI expression could further augment these levels following TGFβ-treatment, while primary tumor cells did not respond to TGFβ (**Figure 2D**). Altogether these results indicated that a functional TGFβ receptor is mandatory for TGFβ-responsiveness, while the contribution of canonical/alternative signaling required further clarification. These considerations led us to propose two different mechanisms for TGFBI secretion in primary CRC and CRC-liver metastasis. While in primary tumors TGFBI levels are maintained by stromal TGFβ-program, in liver metastases TGFBI is also secreted by cancer cells which in turn can respond to TGFβ stimulation.

Different, alternatively wired TGFβ-signaling pathways are responsible for TGFBI induction in CRC cells. Given the fact that SMAD2 was not mutated in TGFβ-responsive CRC cells, we first sought to verify if SMAD2 is required for TGFBI induction. To this end we silenced SMAD2 in HT29hm cells and observed that TGF-β1 can still induce TGFBI expression regardless

of SMAD2 status (**Figure 3A**). Considering that SMAD4 was found mutated in all TGFBI expressing cells, we further hypothesized that a non-canonical signaling pathway may be responsible for the ability of CRC cells to respond to TGF-β1. To clarify this, we have tested if p38, AKT, JNK or MAPK are involved in alternative TGF-β1 signaling in HT29hm cells. As shown in **Figure 3B**, selective inhibitors of p38 (SB202190 and ARRY-614) dampened the TGF-β1-mediated induction of TGFBI in HT29hm cells. In contrast to this, the inhibition of AKT (MK2206) and JNK (SP600125) (**Figure 3C**) could not suppress TGFBI expression following the treatment of HT29hm cells with TGF-β1. The inhibition of MEK1/MEK2 (PD98059) somewhat dampened the responsiveness of HT29hm to TGF-β1, however this was not significant in comparison to TGF-β1 treatment alone (**Figure 3D**). While p38 seems to be relevant to the ability of TGF-β1 to induce TGFBI expression in HT29hm cells, it was unclear how this process may happen given the inability of p38 to function as transcription factor. To this end we sought to test NFKB as this transcription factor has been shown in the past to be able to mediate p38 signaling. Indeed, a selective inhibitor of NFKB (BAY11-7082) reduced TGFBI levels post TGF-β1 stimulation of HT29hm cells, suggesting that NFKB could be in part involved as transcription factor (**Figure 3E**). Following the molecular data showing the importance of p38 – NFKB axis in the TGF-β1 signaling of HT29hm cells, we next verified if the inhibitors of the p38 and NFKB proteins could impinge on the growth and viability of these CRC cells. Both p38 and NFKB inhibitors significantly reduced number of colonies of HT29hm cells (**Figure 3F**), at least in part via regulating the cell viability (**Figure 3G**).

Having acquired evidence that p38 is key for TGFBI expression in HT29hm cells, we next sought to confirm this using SW1222 cells. None of the MAP kinases tested showed the ability to decrease TGFBI expression post TGF-β1 stimulation of SW1222 cells (**Figure S3A-D**). NFKB inhibition could also not reduce the ability of SW1222 cells to respond to TGF-β1 stimulation (**Figure S3E**). In contrast to HT29hm, inhibition of p38 in SW1222 cells caused a strong induction of TGFBI expression that was additionally exacerbated by TGF-β1 treatment (**Figure S3A**). These findings collectively indicate that TGF-β1 signaling is certainly differently wired in different CRC cells and that therapeutic strategies should rather focus on down-stream proteins that assume effector functions. In line with this, we next sought to better understand the function of TGFBI in CRC progression.

TGFBI silencing reduces tumor growth *in vivo* and suppresses angiogenesis *in vitro*. Previous studies have reported a dual role of TGFBI in the progression of many different tumors. In the light of these opposite observations it was important to verify which type of function does TGFBI assume in the present model of CRC. For this purpose, we examined the impact of modulating TGFBI levels on the migration and proliferation of the SW1222 cells. Silencing

TGFBI in SW1222 cells was efficient in reducing their migratory capacity (**Figure S4A-B**) as well as decreased their viability (MTT assay) and ability to form colonies (**Figure S4C-E**). Accordingly, supplementing TGFBI to SW1222 cells increased their proliferation as well as their migration capacity (**Figure S4F-G**). To further understand the putative mechanism, we engaged in the proteomic analysis of SW1222 and HT29 cells following their depletion of TGFBI. We analyzed both intra- and extra-cellular proteins, the latter being collected from the conditioned media. As shown in **Figure S5** (and **Table S4**), particularly up-regulated were proteins involved in JAK-STAT signaling, activation of RAP1 and RAC1 small GTPases as well as in detoxification and photolytic-degradation processes. Down-regulated were proteins involved in particular in metabolism and infectious diseases (**Figure S6** and **Table S4**). Having demonstrated that TGFBI is favoring migration and proliferation of cancer cells *in vitro* we next sought to examine its effects *in vivo*. For this purpose we used two models, one based on CAM tumor development and the second on orthotopic engraftment in mice livers by intrasplenic injection of cancer cells. Silencing *TGFBI* in SW1222 cells reduced tumor growth in the CAM assay (**Figure 4A**) and decreased the development of liver metastases in the orthotopic murine model (**Figure 4B**). Following these *in vivo* experiments, especially the CAM assay, it was evident that the TGFBI depleted tumors displayed a markedly low level of vascularization. This observation led to further *in vitro* experiments aiming at clarifying the potential role of TGFBI in angiogenesis. To this end we recovered conditioned media from control (shNT) and *TGFBI*-silenced SW1222 and HT29 cells and we tested their effect on HUVEC cells. As shown in the **Figure 4C-E**, conditioned media from TGFBI silenced cancer cells significantly decreased the proliferation, migration and sprouting capacity of HUVEC cells. Moreover, supplementing these media with recombinant TGFBI blocked the inhibitory effect, while in the case of sprouting assay the effect was even reversed (**Figure 4E**). Following this observation, we next sought to understand the potential mechanism underlying the pro-angiogenic function of TGFBI. We have resorted to proteomic analysis of HUVEC, which were treated with recombinant TGFBI. As outlined in the **Figures S7-S8** (as well as **Table S4**), recombinant TGFBI in HUVEC activated spliceosome and lysosome related pathways while it decreased processes related to platelet activation, axon guidance and cellular response to stress. Collectively, the data indicated an overall tumor-promoting role of TGFBI in CRC and thus warranted the development of appropriate means to target this protein.

Monoclonal antibodies targeting TGFBI suppress angiogenesis *in vitro* and serve as diagnostic tools *in vivo*. In order to develop novel antibodies against TGFBI we engaged in a *de novo* immunization and screening process. As outlined in **Figure S9A**, nine anti-TGFBI antibodies have been selected, all of which had no cross reactivity to POSTN (**Figure S9B**). Subsequent validations using FACS, WB, SPR and IF analysis have ultimately led to a choice of

two clones, 10G9A10 and 4G6B10, which were further validated *in vitro* (**Figure S9B-E**). Following validation, we next sought to test functionally the selected antibodies for their ability to inhibit angiogenesis using HUVEC cells. For this purpose, HUVEC proliferation and sprouting was monitored after their challenge with CM from SW1222 and HT29hm cells, with or without the presence of anti-TGFBI antibodies. Both clones were able to significantly suppress HUVEC proliferation and sprouting (**Figure 5A**), while this effect was abrogated after antibody denaturation/boiling. Next to therapeutic applications, monoclonal antibodies are also used today in clinical diagnostics. We have thus sought to test if the selected antibodies could qualify as diagnostic tools. To this end we have developed a sandwich ELISA assay based on the two anti-TGFBI clones. We have used this assay to screen sera from CRC patients who were either naïve or were under active chemotherapy treatment. As demonstrated in **Figure 5B**, TGFBI was readily detectable in the serum of both healthy individuals as well as CRC patients (for clinical information see **Table S1**). The latter group had a significantly higher TGFBI serum levels when the patients were untreated, while patients under treatment had comparable levels to normal individuals. Having demonstrated the value of TGFBI antibodies for *in vitro* diagnostics, we next sought to clarify if these could be also used for *in vivo* imaging of liver metastases. To further explore this, we have selected 4G6B10 anti-TGFBI clone because of higher target binding affinity as shown in SPR analysis (**Figure S9D**). Following the antibody labeling using [89]Zr PET tracer, the purified product was injected i.v. in mice bearing either HCT116 or HT29hm liver metastases. The former was used as a negative control knowing that these CRC cells do not express the target. Following injection, PET signal was clearly observable in the CRC-LM of HT29hm mice as early as 2 days post injection (data not shown). The signal intensity reached a maximum at day 6 (**Figure 5C**), and was still detectable on day 14 (data not shown). To further examine the specificity of the signal as well as to gain information on the microscopic distribution, animals bearing HT29hm CRC-LM were injected with either IgG control antibody or anti-TGFBI. Livers were recovered from animals at day 6 post-injection and examined histologically (**Figure 5D**). The results showed a very strong accumulation of the anti-TGFBI antibody especially in the stroma of the liver metastases. Very little to no staining was observed in the HT29hm cells themselves, suggesting that antibodies against TGFBI target cannot be internalized.

DISCUSSION

TGFβ superfamily comprises a large family of different cytokines that include TGF-β, activin, bone morphogenetic proteins (BMPs) and 6 receptors. The latter have varying affinities to groups of ligands and signal downstream in canonical (SMAD-mediated) and non-canonical fashion (ATK, MAPK and others). In the normal colon mucosa, the gradient of BMP/TGFβ levels is

inversely proportional with the differentiation degree of the epithelial cells, and as such is important for the stem cell maintenance in the colon crypts. Our current understanding of TGFβ function in malignant transformation is strongly limited to its tumor inhibiting and tumor promoting functions. Both are viewed as temporally separated processes and solely caused by loss-of-function mutations across the TGFβ superfamily [7]. These events are thought to segregate early versus late steps in CRC development, drawing a line between tumor inhibiting and promoting roles of TGFβ. For example, SMAD4 is mutated in juvenile polyposis patients, predisposing these individuals for diverse gastrointestinal tumors [27]. In CRC, MSI-HI patients present multiple mutations of TGFβ signaling components and have lower TGFβ activity and longer survival times [28]. Speaking for its tumor suppressive role are also recent findings showing that TGFβ downregulates calcium-binding EGF domain-1 (CCBE1) in epithelial cancer cells, which is essential for tumor lymphangiogenesis [29]. However, CRC patients with highest TGFβ activity have the worst clinical prognosis [30]. As cancer cells are mutated for several components of the TGFβ signaling, it is commonly thought that they cannot directly benefit from this potent cytokine. Thus, a model has been developed (largely based on animal studies) where CAF orchestrate pro-tumorigenic TGFβ program in CRC [8]. In this model, TGFβ activates SMAD3 in the CAF, which in turn produce several pro-metastatic factors such as ANGPTL4, PTHLH, CTGF or JAG1. In the light of these results targeting TGFβ should represent a veritable treatment opportunity, especially in the late phase of tumor development. However, clinical trials with various TGFβ inhibitors have proven rather disappointing across different malignancies including colorectal cancer [31]. This is a strong indicator that tumor inhibiting and promoting functions of TGFβ cannot be separated in time, suggesting that cell-type specific pro- and anti-tumor wiring of the pathway needs to be fundamentally revisited.

In the frame of the present work we focus on TGFBI, a protein that evidences activation of TGFβ pathway across different cell models. In colon, TGFBI has been identified as a marker gene that distinguishes normal mucosa from benign adenoma and colon cancer in humans [32]. Its increasing mRNA expression positively correlated with the transition from normal to cancer. We and others have repeatedly found significant up-regulation of TGFBI in the colon tumors and associated metastases [17, 22, 33]. A plethora of data implicates TGFBI in tumoral progression. However, surprisingly very little is known regarding its relationship with TGFβ – beyond the fact that TGFβ induces TGFBI expression. This is indeed primordial in order to understand the role of TGFBI in early aspects of tumor progression. *Tgfbi* knockout mice are predisposed to multiple cancer formation including CRC [16] as well as alterations in cartilage and bone formation [34]. This in turn suggests that basal levels of TGFBI, such as frequently seen in the fibroblasts of normal colon, are required for homeostatic function of TGFβ. In normal colon TGFβ is produced

by resident fibroblasts for autocrine and paracrine purposes. TGFβ activity in fibroblasts stimulates ECM production and the formation of the basement membrane. The latter serves as an important support for the epithelial cells, contributing to epithelial polarity [35]. TGFBI might in particular be implicated in this process. However, the role of TGFBI in the physiology of the normal colon remains to be clarified in future studies. We critically show here that TGFBI expressed by metastatic CRC cells serves a pro-tumorigenic function. The latter affects the crosstalk between cancer and endothelial cells, resulting in enhanced angiogenesis.

An important feature that may clarify the role of TGFBI in colon cancer is probably related to the upstream signaling that controls its expression. Namely, a handful of human studies have for nearly two decades reported on responsiveness of CRC epithelial cells to TGFβ, despite numerous mutations in the downstream signaling machinery [11, 36, 37]. If TGFβ functionality in the tumor epithelium was actually never completely lost, then it is intriguing to ask the question how TGFβ tumor suppressor function was rewired to tumor promoter. Before attempting to do so, it is worth taking a look at other much more aggressive human tumors, such as melanoma or glioblastoma. In those particular instances TGFβ signaling is maintained in cancer cells and is mainly facilitated by non-canonical signaling through PI3K/AKT and RAS/MAPK pathways [38]. In these tumors, canonical SMAD-dependent signaling can also contribute to pro-metastatic functions, in particular by up-regulating pro-EMT genes *SLUG* and *SNAIL* [39, 40]. In the present work, we show that TGFBI signaling follows an alternative, non-canonical pathway that at least in some cases relies on p38. Additionally, mutation in p53 appears to raise the basal levels of TGFBI protein while not directly affecting the amplitude of TGFβ response. Our data do not exclude that other non-canonical pathways are certainly equally essential, yet their identity remains to be unveiled. While this process may help the development of new therapeutic strategies for CRC patients, their implementation will inevitably require personalized medicine. Indeed, as shown here, not all cancer cells (and most probably not all patients) will follow the same alternative TGFβ-signaling pathway. In the light of this mechanistic complexity, targeting the effector proteins that result from this alternative signaling might be a more promising strategy. Our study reinforces previous findings that TGFBI is certainly one of such targets in colon cancer. Importantly, we show for the first time that TGFBI is accessible to therapeutic antibodies *in vivo*, and relate its function to induction of angiogenesis. Future studies should examine how more potent anti-TGFBI antibodies can be put in place to achieve a stronger functional effect. In addition, one should explore the combination of these TGFBI targeting strategies with other therapies that affect other hallmarks of cancer such as proliferation, metabolism or immunity.

ACKNOWLEDGEMENTS

REFERENCES

1. Engstrand J, Nilsson H, Stromberg C, Jonas E, Freedman J. Colorectal cancer liver metastases - a population-based study on incidence, management and survival. BMC Cancer. 2018; 18: 78.

2. Sosa MS, Bragado P, Aguirre-Ghiso JA. Mechanisms of disseminated cancer cell dormancy: an awakening field. Nat Rev Cancer. 2014; 14: 611-22.

3. Massague J, Obenauf AC. Metastatic colonization by circulating tumour cells. Nature. 2016; 529: 298-306.

4. Hanahan D, Coussens LM. Accessories to the crime: functions of cells recruited to the tumor microenvironment. Cancer Cell. 2012; 21: 309-22.

5. Ronca R, Van Ginderachter JA, Turtoi A. Paracrine interactions of cancer-associated fibroblasts, macrophages and endothelial cells: tumor allies and foes. Curr Opin Oncol. 2018; 30: 45-53.

6. Oft M, Peli J, Rudaz C, Schwarz H, Beug H, Reichmann E. TGF-beta1 and Ha-Ras collaborate in modulating the phenotypic plasticity and invasiveness of epithelial tumor cells. Genes Dev. 1996; 10: 2462-77.

7. Jung B, Staudacher JJ, Beauchamp D. Transforming growth factor beta superfamily signaling in development of colorectal cancer. Gastroenterology. 2017; 152: 36-52.

8. Calon A, Espinet E, Palomo-Ponce S, Tauriello DV, Iglesias M, Cespedes MV, et al. Dependency of colorectal cancer on a TGF-beta-driven program in stromal cells for metastasis initiation. Cancer Cell. 2012; 22: 571-84.

9. Xu Y, Pasche B. TGF-beta signaling alterations and susceptibility to colorectal cancer. Hum Mol Genet. 2007; 16 Spec No 1: R14-20.

10. Luo J, Chen XQ, Li P. The role of TGF-beta and its receptors in gastrointestinal cancers. Transl Oncol. 2019; 12: 475-84.

11. de Miranda NF, van Dinther M, van den Akker BE, van Wezel T, ten Dijke P, Morreau H. Transforming growth factor beta signaling in colorectal cancer cells with microsatellite instability despite biallelic mutations in TGFBR2. Gastroenterology. 2015; 148: 1427-37 e8.

12. Skonier J, Neubauer M, Madisen L, Bennett K, Plowman GD, Purchio AF. cDNA cloning and sequence analysis of beta ig-h3, a novel gene induced in a human adenocarcinoma cell line after treatment with transforming growth factor-beta. DNA Cell Biol. 1992; 11: 511-22.

13. Huber O, Sumper M. Algal-CAMs: isoforms of a cell adhesion molecule in embryos of the alga Volvox with homology to Drosophila fasciclin I. EMBO J. 1994; 13: 4212-22.

14. Nieberler M, Reuning U, Reichart F, Notni J, Wester HJ, Schwaiger M, et al. Exploring the role of RGD-recognizing integrins in cancer. Cancers (Basel). 2017; 9.

15. Yokobori T, Nishiyama M. TGF-beta signaling in gastrointestinal cancers: progress in basic and clinical research. J Clin Med. 2017; 6.

16. Zhang Y, Wen G, Shao G, Wang C, Lin C, Fang H, et al. TGFBI deficiency predisposes mice to spontaneous tumor development. Cancer Res. 2009; 69: 37-44.

17. Ma C, Rong Y, Radiloff DR, Datto MB, Centeno B, Bao S, et al. Extracellular matrix protein betaig-h3/TGFBI promotes metastasis of colon cancer by enhancing cell extravasation. Genes Dev. 2008; 22: 308-21.

18. Waltregny D, Bellahcene A, Van Riet I, Fisher LW, Young M, Fernandez P, et al. Prognostic value of bone sialoprotein expression in clinically localized human prostate cancer. J Natl Cancer Inst. 1998; 90: 1000-8.

19. Grillet F, Bayet E, Villeronce O, Zappia L, Lagerqvist EL, Lunke S, et al. Circulating tumour cells from patients with colorectal cancer have cancer stem cell hallmarks in ex vivo culture. Gut. 2017; 66: 1802-10.

20. Giraud J, Failla LM, Pascussi JM, Lagerqvist EL, Ollier J, Finetti P, et al. Autocrine secretion of progastrin promotes the survival and self-renewal of colon cancer stem-like cells. Cancer Res. 2016; 76: 3618-28.

21. Schindelin J, Arganda-Carreras I, Frise E, Kaynig V, Longair M, Pietzsch T, et al. Fiji: an open-source platform for biological-image analysis. Nat Methods. 2012; 9: 676-82.

22. Turtoi A, Blomme A, Debois D, Somja J, Delvaux D, Patsos G, et al. Organized proteomic heterogeneity in colorectal cancer liver metastases and implications for therapies. Hepatology. 2014; 59: 924-34.

23. Kilkenny C, Browne WJ, Cuthill IC, Emerson M, Altman DG. Improving bioscience research reporting: the ARRIVE guidelines for reporting animal research. PLoS Biol. 2010; 8: e1000412.

24. Vosjan MJ, Perk LR, Visser GW, Budde M, Jurek P, Kiefer GE, et al. Conjugation and radiolabeling of monoclonal antibodies with zirconium-89 for PET imaging using the bifunctional chelate p-isothiocyanatobenzyl-desferrioxamine. Nat Protoc. 2010; 5: 739-43.

25. Price JE, Daniels LM, Campbell DE, Giavazzi R. Organ distribution of experimental metastases of a human colorectal carcinoma injected in nude mice. Clin Exp Metastasis. 1989; 7: 55-68.

26. Cordenonsi M, Dupont S, Maretto S, Insinga A, Imbriano C, Piccolo S. Links between tumor suppressors: p53 is required for TGF-beta gene responses by cooperating with Smads. Cell. 2003; 113: 301-14.

27. Johansson J, Sahin C, Pestoff R, Ignatova S, Forsberg P, Edsjo A, et al. A novel SMAD4 mutation causing severe juvenile polyposis syndrome with protein losing enteropathy, immunodeficiency, and hereditary haemorrhagic telangiectasia. Case Rep Gastrointest Med. 2015; 2015: 140616.

28. Watanabe T, Wu TT, Catalano PJ, Ueki T, Satriano R, Haller DG, et al. Molecular predictors of survival after adjuvant chemotherapy for colon cancer. N Engl J Med. 2001; 344: 1196-206.

29. Song J, Chen W, Cui X, Huang Z, Wen D, Yang Y, et al. CCBE1 promotes tumor lymphangiogenesis and is negatively regulated by TGFβ signaling in colorectal cancer. Theranostics. 2020; 10: 2327-41.

30. Guinney J, Dienstmann R, Wang X, de Reynies A, Schlicker A, Soneson C, et al. The consensus molecular subtypes of colorectal cancer. Nat Med. 2015; 21: 1350-6.

31. Neuzillet C, Tijeras-Raballand A, Cohen R, Cros J, Faivre S, Raymond E, et al. Targeting the TGFbeta pathway for cancer therapy. Pharmacol Ther. 2015; 147: 22-31.

32. Buckhaults P, Rago C, St Croix B, Romans KE, Saha S, Zhang L, et al. Secreted and cell surface genes expressed in benign and malignant colorectal tumors. Cancer Res. 2001; 61: 6996-7001.

33. Greening DW, Kapp EA, Ji H, Speed TP, Simpson RJ. Colon tumour secretopeptidome: insights into endogenous proteolytic cleavage events in the colon tumour microenvironment. Biochim Biophys Acta. 2013; 1834: 2396-407.

34. Yu H, Wergedal JE, Zhao Y, Mohan S. Targeted disruption of TGFBI in mice reveals its role in regulating bone mass and bone size through periosteal bone formation. Calcif Tissue Int. 2012; 91: 81-7.

35. Stahl PJ, Felsen D. Transforming growth factor-beta, basement membrane, and epithelial-mesenchymal transdifferentiation: implications for fibrosis in kidney disease. Am J Pathol. 2001; 159: 1187-92.

36. Ilyas M, Efstathiou JA, Straub J, Kim HC, Bodmer WF. Transforming growth factor beta stimulation of colorectal cancer cell lines: type II receptor bypass and changes in adhesion molecule expression. Proc Natl Acad Sci U S A. 1999; 96: 3087-91.

37. Baker K, Raut P, Jass JR. Microsatellite unstable colorectal cancer cell lines with truncating TGFbetaRII mutations remain sensitive to endogenous TGFbeta. J Pathol. 2007; 213: 257-65.

38. Zhang L, Zhou F, ten Dijke P. Signaling interplay between transforming growth factor-beta receptor and PI3K/AKT pathways in cancer. Trends Biochem Sci. 2013; 38: 612-20.

39. Moustakas A, Heldin CH. Mechanisms of TGFbeta-induced epithelial-mesenchymal transition. J Clin Med. 2016; 5.

40. Chen Y, Liu P, Sun P, Jiang J, Zhu Y, Dong T, et al. Oncogenic MSH6-CXCR4-TGFB1 feedback loop: a novel therapeutic target of photothermal therapy in glioblastoma multiforme. Theranostics. 2019; 9: 1453-73.
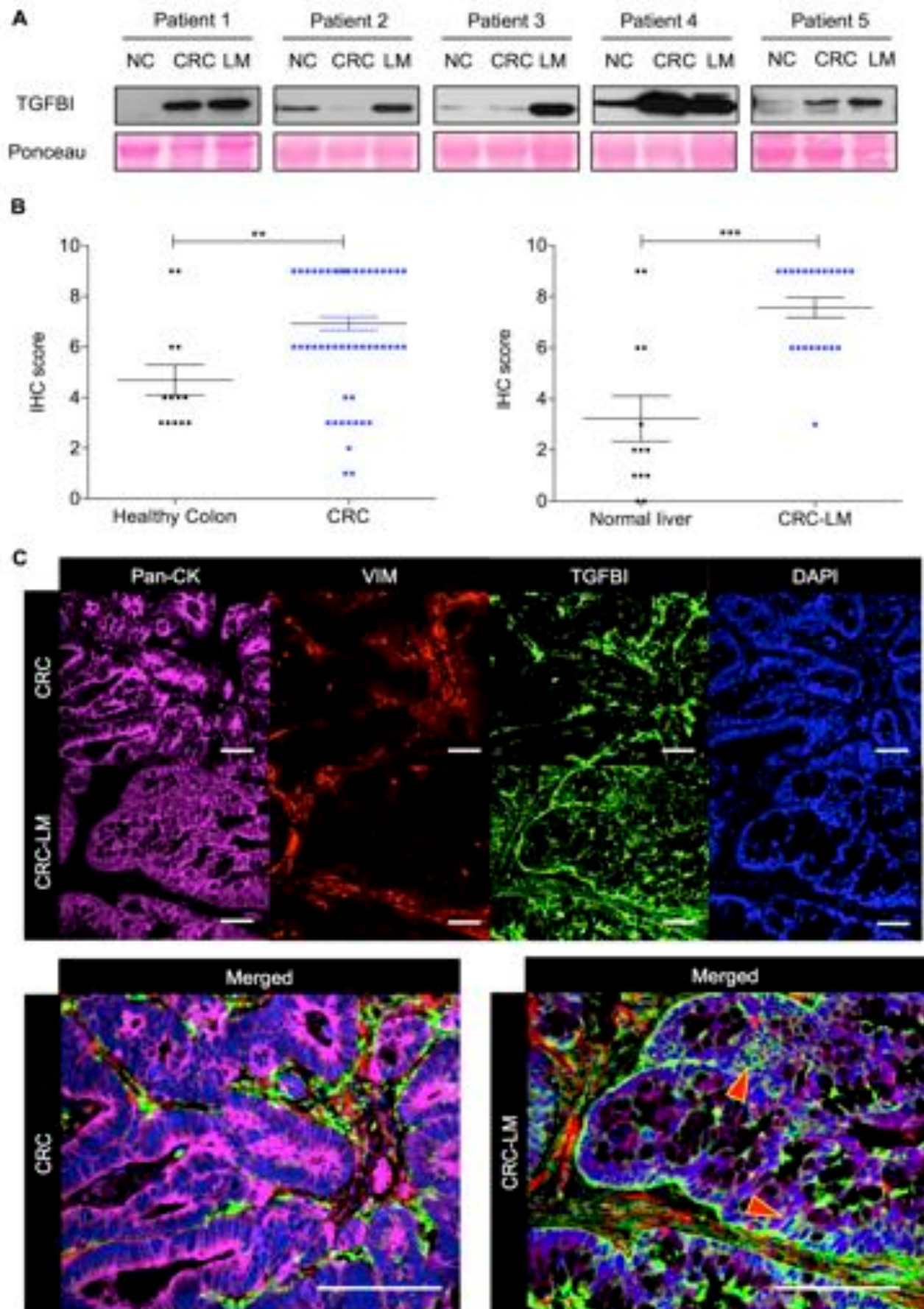
Figure Legends

A

B

C

Figure 1: TGFBI is strongly expressed in CRC and CRC-LM human tumors. **A**. Western blot analysis of TGFBI expression profile in tissue extracts from normal colon, CRC and matched CRC-LM from 5 different patients. Ponceau Red staining was used for normalization. **B**. Immunohistochemical analysis of TGFBI expression in CRC (n=78) and CRC-LM (n=21) patients. Adjacent normal colon and normal liver tissues, when available, served as controls (** and *** indicate $p<0.01$ and $p<0.001$ respectively; error bars are standard deviation of means). **C**. IF analysis of TGFBI expression in CRC and CRC-LM specimens, co-stained with pan-cytokeratin (cancer cells), vimentin (stromal cells) and DAPI (nuclei). Shown are representative pictures of 20 cases.
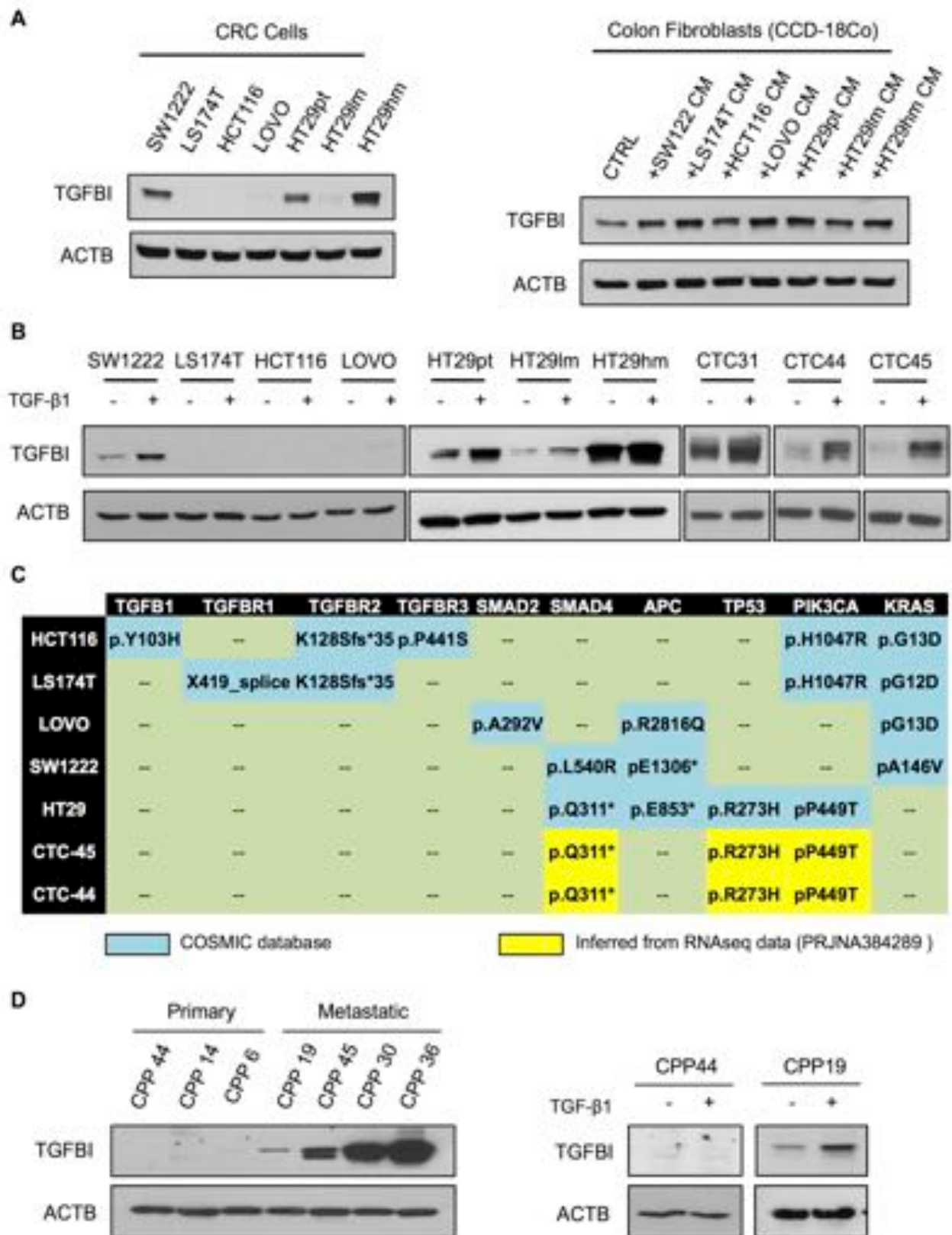
Figure 2: Metastatic CRC cells maintain TGFβ-signaling. **A**. Western blot analysis of TGFBI expression in a set of commercially available CRC cell lines (left panel) and in normal colon fibroblasts (CCD-18Co) treated or not with conditioned media of CRC cells (right panel). ACTB was used for normalization. **B**. Western blot analysis of TGF-β1-responsiveness of CRC cells and

human CTC. **C**. Table showing the mutation profile of key components of TGFβ-signaling and tumor driver genes in CRC and CTC cells (CTC31 no sequencing information available). All cells were WT for SMAD3 and NRAS. **D**. Basal expression of TGFBI in human primary and metastatic CRC cells (left panel). TGFBI expression levels in primary and metastatic CRC cells from 2 different patients under TGF-β1 stimulation. Panels A, B and D are representative gels from three biological replicates.
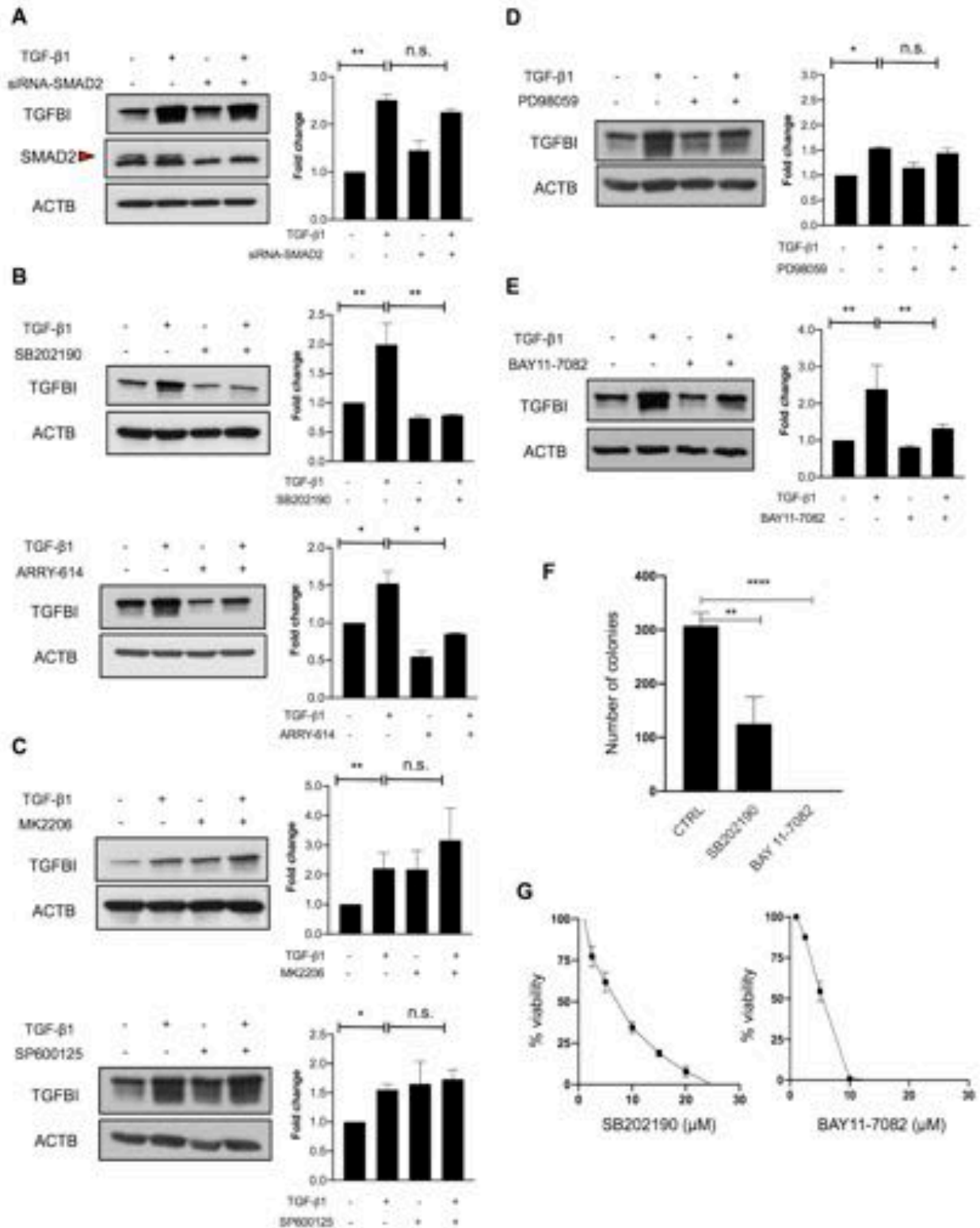
Figure 3: Alternative TGFβ-signaling in CRC is at least in part driven by p38. **A**. Western blot analysis of TGFBI expression in HT29hm cells treated with TGF-β1 following the silencing of SMAD2. ACTB as loading control. **B**. TGFBI protein levels in HT29hm cells after treatment with TGF-β1 (5 ng/ml) and SB202190 (5 μM) or ARRY-614 (10 μM) p38 inhibitors, alone or in

combination for 48 h. **C.** Same as in panel (**B**), instead of p38 inhibitors MK2206 (1 µM, AKT inhibitor), SP600125 (5 µM, JNK inhibitor). **D.** TGFBI expression in HT29hm cells after treatment with TGF-β1 and PD98059 (5 µM, MAPK inhibitor). **E.** Same as in panel (**B**) with BAY11-7082 (5 µM, NFKB inhibitor). Panels A-E: shown are representative gels from three biological replicates. **F.** Colony formation assay with HT29hm cells following their concomitant treatment with p38 and NFKB inhibitors, SB202190 and BAY11-7082 respectively. **G.** HT29hm viability following the treatment with same inhibitors as in **F**. Panels **F** and **G** show average values resulting from biological triplicates. All panels: */** denote statistical significance with p<0.05 and p<0.01 respectively, n.s. stands for non-significant and error bars represent standard deviation of means.
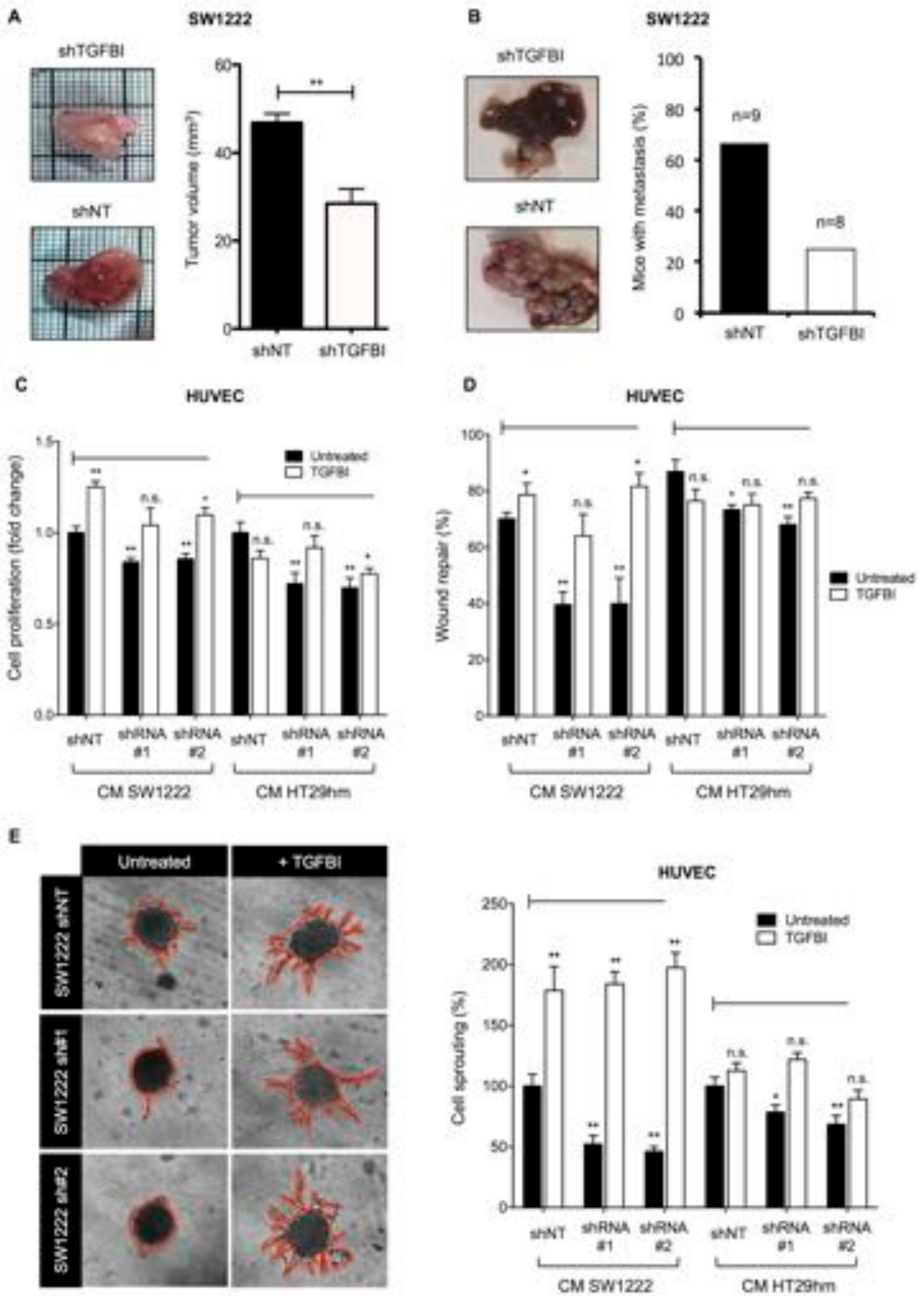
Figure 4: TGFBI promotes tumor growth and angiogenesis. **A**. CAM angiogenesis/tumor development model using SW1222 cells silenced for *TGFBI* or scrambled shRNA and quantification of the tumor volume. **B**. Orthotopic liver metastasis model using the same cells as in (**A**). **C**. Proliferation and **D**. wound healing assays using HUVEC incubated with conditioned media of SW1222 and HT29 cells silenced for TGFBI or scramble shRNA, treated or not with recombinant TGFBI. **E**. Sprouting assay using HUVEC; same conditions as panel (**C**) and (**D**). Panels **A**, **C-E**: graphs represent averages of quadruplicate biological experiments while */** denote statistical significance with $p < 0.05$ and $p < 0.01$ respectively (treatment conditions compared to untreated shNT); n.s. stands for non-significant; error bars are standard deviations of means.
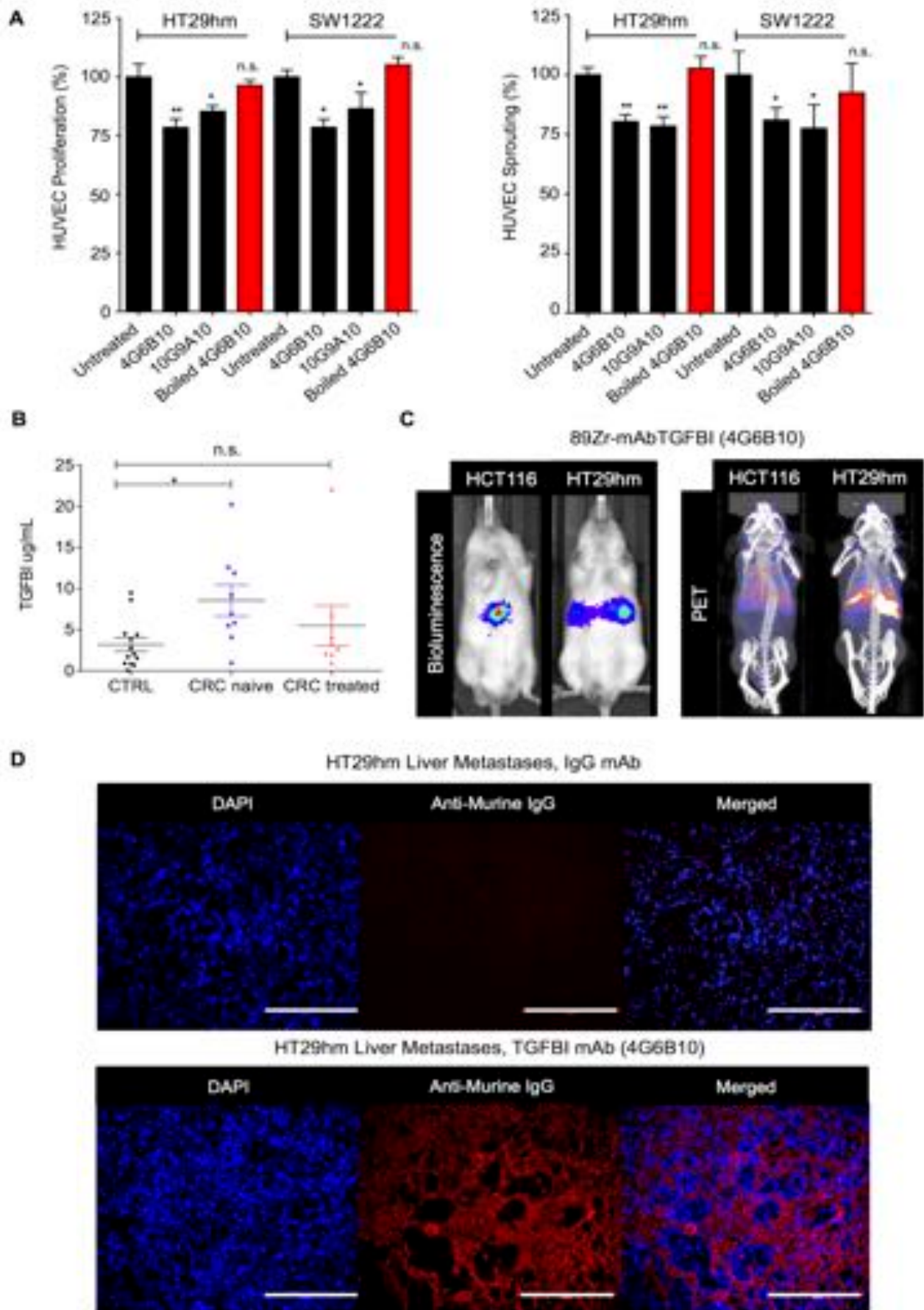
A

B

C

89Zr-mAbTGFBI (4G6B10)

D

HT29hm Liver Metastases, IgG mAb

HT29hm Liver Metastases, TGFBI mAb (4G6B10)

Figure 5: TGFBI is a diagnostic marker for CRC-LM. **A.** Targeting proliferation and sprouting of HUVEC cells using specific anti-TGFBI antibodies *in vitro*. **B.** Quantification of TGFBI levels using ELISA based on 4G6B10 and 10G9A10 anti-TGFBI antibodies, in sera from healthy individuals and CRC patients treated or not with chemotherapy (N=9 naïve CRC, 8 treated CRC and 15 healthy patients; for further details see **Table S1**). **C.** Comparison between bio-luminescence (left) and PET/CT (right) imaging using ^{89}Zr-radiolabeled 4G6B10 mAb (day 6) in mice with liver metastasis xenografts. **D.** Ex-vivo detection of 4G6B10 antibody or irrelevant IgG following their i.v. injection in the HT29hm orthotopic mouse model (shown are representative images of 5 animals/group). Panels **A** and **B**: indicated are average values resulting from biological triplicates; */** denote statistical significance with $p<0.05$ and $p<0.01$ respectively, n.s. stands for non-significant and error bars represent standard deviation of means. Panels **C** and **D**: shown are representative images of 4 biological replicates.
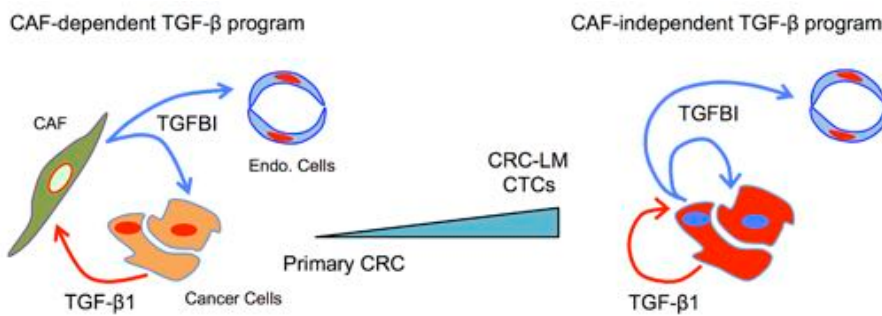
Graphical abstract: Model of TGFβ-orchestrated pro-angiogenic program in primary CRC and in CRC-LM. TGFBI secretion switches from CAF to cancer in the process of metastasis. Metastatic and circulating cancer cells become CAF-independent.